The Astrophysical Journal, 906:46 (8pp), 2021 January 1 https://doi.org/10.3847/1538-4357/abc690

A New Method to Estimate Halo CME Mass Using Synthetic CMEs Based on a Full Ice Cream Cone Model

Hyeonock Na[1], Yong-Jae Moon[1,2], Jin-Yi Lee[2], and Il-Hyun Cho[2]
[1] School of Space Research, Kyung Hee University, Yongin, 17104, Republic of Korea; moonyj@khu.ac.kr
[2] Department of Astronomy and Space Science, College of Applied Science, Kyung Hee University, Yongin, 17104, Republic of Korea
Received 2020 June 24; revised 2020 October 11; accepted 2020 October 29; published 2021 January 5

Abstract

In this study, we suggest a new method to estimate the mass of a halo coronal mass ejection (CME) using synthetic CMEs. For this, we generate synthetic CMEs based on two assumptions: (1) the CME structure is a full ice cream cone, and (2) the CME electron number density follows a power-law distribution ($\rho_{\mathrm{cme}} = \rho_0 r^{-n}$). The power-law exponent n is obtained by minimizing the rms error between the electron number density distributions of an observed CME and the corresponding synthetic CME at a position angle of the CME leading edge. By applying this methodology to 56 halo CMEs, we estimate two kinds of synthetic CME masses. One is a synthetic CME mass that considers only the observed CME region (M_{cme1}), the other is a synthetic CME mass that includes both the observed CME region and the occulted area (M_{cme2}). From these two cases, we derive conversion factors that are the ratio of a synthetic CME mass to an observed CME mass. The conversion factor for M_{cme1} ranges from 1.4 to 3.0 and its average is 2.0. For M_{cme2}, the factor ranges from 1.8 to 5.0 with an average of 3.0. These results imply that the observed halo CME mass can be underestimated by about 2 times when we consider the observed CME region, and about 3 times when we consider the region including the occulted area. Interestingly these conversion factors have a very strong negative correlation with angular widths of halo CMEs.

Unified Astronomy Thesaurus concepts: Solar coronal mass ejections (310); Solar corona (1483)

1. Introduction

Coronal mass ejections (CMEs) are very explosive phenomena of the Sun and are well known as causes of geomagnetic storms (e.g., Gosling et al. 1991). It is important to understand their three-dimensional kinematics (e.g., mass, velocity, angular width, and source location) for space weather forecasts. The CMEs are commonly observed in white-light coronagraphs such as the Large Angle and Spectrometric Coronagraph (LASCO; Brueckner et al. 1995) on board the Solar and Heliospheric Observatory (SOHO; Domingo et al. 1995). Since 1995, SOHO/LASCO has provided us with a large data set of CME images. However, because the observations are projected on the plane of the sky, there may be significant differences between real CME parameters and the observed ones. For a limb CME, the influence of the projection effect is minimal because its propagation direction is near the plane of the sky, while the projection effect for a halo CME (Howard et al. 1982), which propagates toward the Earth, is significantly larger.

Many methods have been presented to estimate the three-dimensional parameters of halo CMEs by minimizing the projection effect. We can estimate parameters such as velocity, angular width, and source location by using a model assuming CME structures such as a cone shape (e.g., Xie et al. 2004; Xue et al. 2005; Michalek 2006; Millward et al. 2013; Na et al. 2017), a graduated cylindrical shell model (Thernisien et al. 2009), or a triangulation method (e.g., Mierla et al. 2008; Liewer et al. 2009; Liu et al. 2010). Even though we adopt such a specific method, it is very hard to estimate the CME mass.

The CME mass is estimated from the coronal brightness by Thomson scattering. For this, we use the assumption that all electrons lie on the plane of the sky, because the brightness measured from the observation does not include the information of the electron distribution due to the projection effect. This mass is typically underestimated by about a factor of 2 (e.g., Vourlidas et al. 2000; Lugaz et al. 2005; Colaninno & Vourlidas 2009). The underestimation may strongly depend on the position of the CME source region.

To estimate more accurate CME mass, many methods have been presented. If we have information related to the source locations of a CME, we can calculate the CME mass using the simple assumption that all electrons of the CME are confined to the plane along the propagating direction (Vourlidas et al. 2010). However, this assumption may significantly overestimate the CME mass when its propagating direction is near the Sun–Earth line such as halo CMEs. After the launch of the Solar Terrestrial Relations Observatories (STEREO; Kaiser et al. 2008), it became possible to estimate a more accurate mass using simultaneously observed data from different points of view. Several studies (e.g., Colaninno & Vourlidas 2009; Bein et al. 2013; de Koning 2017) suggest a method estimating CME mass from the difference of the mass results measured at two or three vantage points. Pluta et al. (2019) presented a method that combines a geometrical model (the GCS model) with the above assumption presented by Vourlidas et al. (2010). Unfortunately, it is difficult to steadily obtain applicable data from different points of view since SOHO/LASCO C3 and the Sun–Earth Connection Coronal and Heliospheric Investigation (SECCHI; Howard et al. 2008) COR2 on board the STEREO have different observation times and cadences. Dai et al. (2015) presented a method using polarization measurements, without other information such as source location or multiview observations. However, it is difficult to continuously apply the SOHO/LASCO C3 data because it does not provide the polarization measurements every observation time, unlike the STEREO/SECCHI COR2.

In this study, we suggest a new method to estimate a halo CME mass using a synthetic CME. To generate synthetic CMEs, we use the following two assumptions. The first assumption is that the CME structure is a full ice cream cone.

Na et al. (2017) presented that the structure of a halo CME observed at an orthogonal direction to its propagating direction is close to the full ice cream cone structure. The second assumption is that the CME electron number density distribution has a power-law distribution. Howard & Vourlidas (2018) showed that the electron number density distributions for the front part of CMEs with a three-part structure follow a power law with an exponent of −3. We determine the power-law exponent by minimizing the difference between density distributions of observations and synthetic ones at a measurement position angle (MPA), which is the position angle corresponding to a portion of the CME leading edge. Then all Thompson scattering contributions of the synthetic CME are calculated. From the synthetic CME, we consider two kinds of CME masses. One is a synthetic CME mass, which considers only the observed CME region, and the other is a synthetic CME mass, which includes both the observed CME region and the occulted area. The mass of the occulted area is estimated from the assumed density distribution but only considering the area with a radial distance larger than 4 solar radii ($R_{\odot}$). If we observe a limb CME in the LASCO C3 field of view, we can identify the CME structure over the occultation disk of LASCO C3. The below parts of the CME are still unknown. From this fact, we consider the area with the radial distance larger than $4\,R_{\odot}$. From these two cases, we derive conversion factors, which are the ratio of a synthetic CME mass to an observed CME mass. We apply this method to 56 halo CMEs observed by SOHO/LASCO C3 from 2000 January to 2014 September and examine the dependence of conversion factors on their three-dimensional parameters. Our method has a couple of advantages over other methods. First, we can apply our method to most of the CMEs (including halo CMEs) that can be applied to a full ice cream cone model. Second, our method needs only total brightness data from single-view observations.

This study is organized as follows. In Section 2, we describe the data used in this study and a method to generate synthetic CMEs and conversion factors. Section 3 presents the results and a discussion. A summary and conclusion are given in Section 4.

2. Data and Method

2.1. Data

In this study, we consider the halo CMEs observed by SOHO/LASCO from 2000 January to 2014 September. During this period, 575 halo CMEs were recorded in the SOHO/LASCO CME catalog (http://cdaw.gsfc.nasa.gov/CME_list). We exclude events with the following conditions: (1) poor events whose boundaries are not very clear in the LASCO/C3 field of view, (2) events observed in only C2 field of view, (3) overlapping events where there are multiple CMEs in a single field of view, (4) events with negative mass, (5) events with less than four observations, and (6) poor pre-event observations. Finally, we select 56 halo CMEs.

2.2. Method

In this study, we present a method to estimate halo CME mass using a synthetic CME. To generate a synthetic CME, we have two assumptions: (1) the CME structure is a full ice cream cone, and (2) the CME electron number density has a power-law distribution, $\rho_{\rm cme} = \rho_0 r^{-n_{\rm cme}}$, where ρ_0 is a constant. Thus, all CME materials are distributed in a full ice cream cone with the power-law density distribution only depending on radial height. To determine the density distribution of the synthetic CME corresponding to the observation, we compare the number densities of the sector at MPA obtained from the observation and the synthetic CME. The detailed process is as follows (for a summary see Figure 1).

Step 1: We determine three-dimensional parameters (radial height r, radial velocity V_r, angular width α, colatitude θ, and longitude ϕ) of a CME using a full ice cream cone model (Na et al. 2017), which assumes that a CME structure is a full ice cream cone, which is a flat cone combined with a hemisphere. We note that there is the degeneracy problem of the parameters from the cone models based on the single-view observation (Millward et al. 2013). As mentioned in Millward et al. (2013), for the same projected structure, it is possible to estimate multiple solutions, for example, a large radial velocity with a small angular width or a small radial velocity with a large angular width. To minimize the problem, we use two additional conditions: (1) the position angle, with maximum projection speed estimated from the model, is located near that of the observation, and (2) a radial velocity from the model is larger than the maximum projection speed of the observation. The full ice cream cone model determines cone model parameters by minimizing the rms error between projection speeds at position angles from the observations and the model. The projection speed at a position angle estimated from the model is defined by the following equation.

$$V_p = V_r \cos\delta(\psi, \alpha, \theta, \phi), \tag{1}$$

where V_p is the projection speed, δ is an angle between the generatrix of the cone and the plane of the sky, and ψ is the position angle of the projection of the generatrix. The detailed description is given by Na et al. (2017). The rms error minimization can find a single solution of the cone model parameters for a CME event as shown in Figure 2. The parameters of the model are used to generate the CME structure.

Step 2: We measure the observed mass of the CME, $M_{\rm obs}$, from a base difference image (CME image—pre-event image). In this study, the CME region projected on the plane of the sky is defined as the projection of the full ice cream cone constructed by the three-dimensional parameters obtained from Step 1. The region is also used for generating the synthetic CME image corresponding to the observation. The observed mass in the region is estimated by a typical method based on an assumption that all electrons lie on the plane of the sky (refer to Vourlidas et al. 2010).

Step 3: From the observation, we estimate the electron number density, $\rho_{\rm os}$, of the spherical sector with 5° angular width at MPA (hereafter MPA sector), which is a position angle corresponding to the portion of the CME leading edge. Here the density and the volume in the MPA sector are given by

$$\rho_{\rm os}(r_{\rm sec}) = \frac{m_{\rm os}(r_{\rm sec})}{V_{\rm sec}} \div m_e, \tag{2}$$

$$V_{\rm sec} = \frac{2}{3}\pi (r_{\rm sec}^{-3} - r_{\rm occ}^{-3})(1 - \cos\alpha_{\rm sec}), \tag{3}$$

where $\rho_{\rm os}$ is the density of the MPA sector, $m_{\rm os}$ is the mass of the MPA sector, $r_{\rm sec}$ is the height of the MPA sector, $V_{\rm sec}$ is the

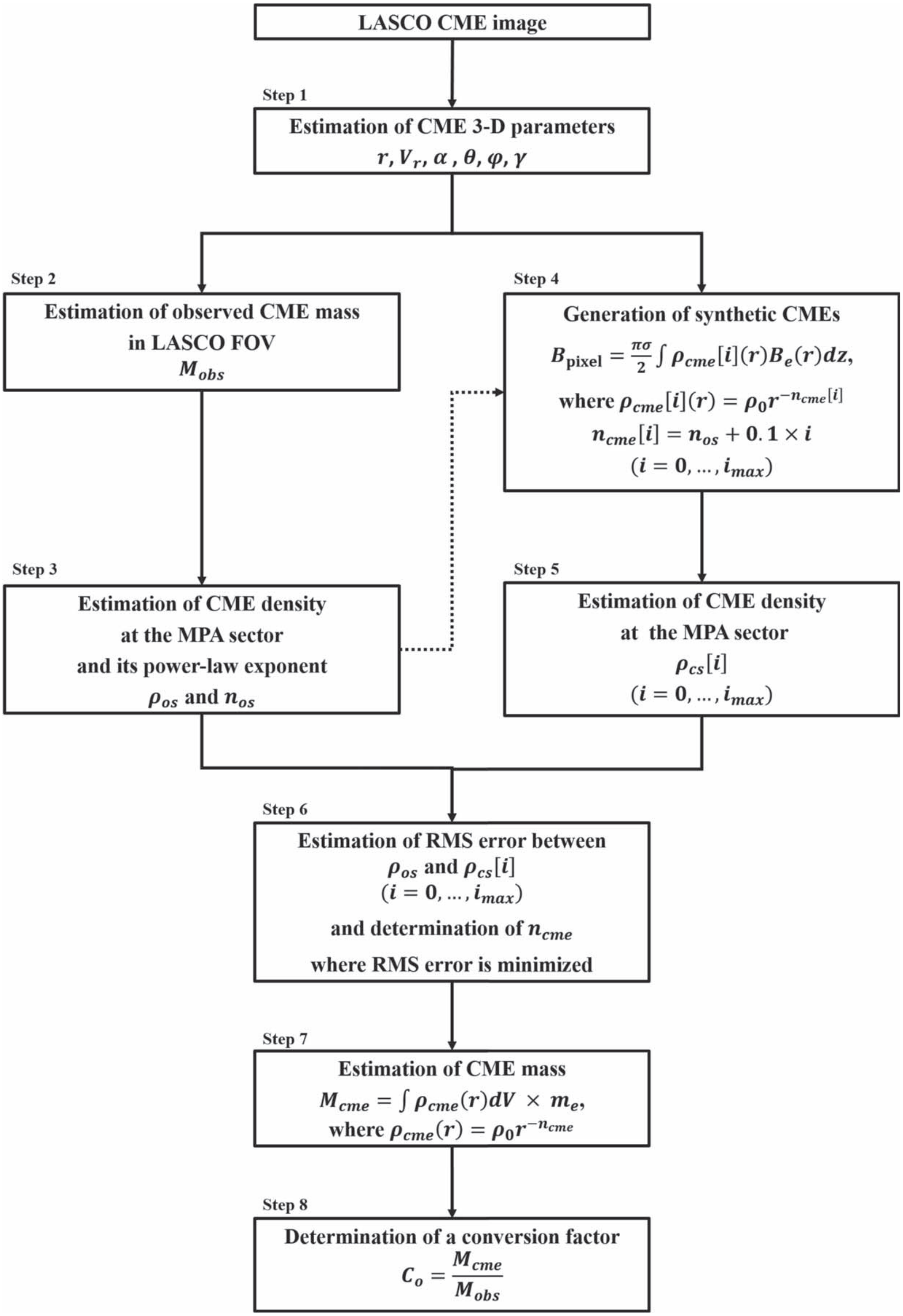

Figure 1. Flowchart of how to determine the mass of a halo CME.

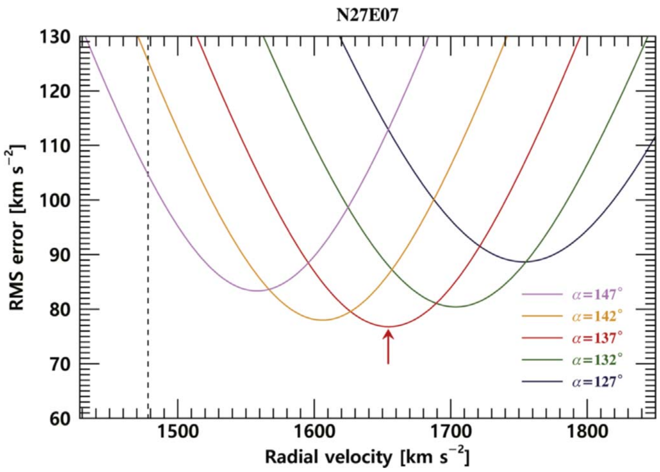

Figure 2. rms error profiles as a function of radial velocity for several angular widths at N27E07 for the 2001 November 17 event. The dashed black line is the maximum projection speed (1478 km s^{-1}) measured from the observation. The red arrow indicates the minimum rms error. In this case, the radial velocity is estimated as 1654 km s^{-1}.

volume of the MPA sector, $r_{\rm occ}$ is the height of the occulter, and $\alpha_{\rm sec}$ is the angular width of the MPA sector. m_e is an effective mass per electron from an assumption that the CME materials comprise 90% hydrogen and 10% helium (1.97×10^{-24} g per electron; Hildner et al. 1975). Then we obtain an power-law exponent $n_{\rm os}$ from a power-law fitting of the density of the MPA sector as a function of height, $\rho_{\rm os} = \rho_{\rm os0} r_{\rm sec}^{-n_{\rm os}}$, where $\rho_{\rm os0}$ is constant.

Step 4: We generate synthetic CMEs based on a full ice cream cone model with a power-law density distribution, $\rho_{\rm cme} = \rho_0 r^{-n_{\rm cme}}$, where ρ_0 is a constant. The total brightness of a pixel, $B_{\rm pixel}$, is estimated by the following equation:

$$B_{\rm pixel} = \frac{\pi\sigma}{2}\int_{\rm LOS} \rho_{\rm cme}(r) B_{\rm e}(r) dz, \tag{4}$$

where σ is the Thomson cross-section used by Billings (1966), r is the distance from the center of the Sun to the scattering location on the line of sight (LOS), z is the distance from the scattering location to the observer, $\rho_{\rm cme}$ is the electron number density at the location, and $B_{\rm e}$ is the brightness of a single electron at the location (e.g., Billings 1966; Howard & Tappin 2009; de Koning 2017). The LOS boundaries are determined by the intersection of the full ice cream cone and the line from the pixel to the observer. Then we estimate the total brightness for all pixels in the CME region that was defined in Step 2. We generate a set of synthetic CMEs by changing the power-law exponent from $n_{\rm cme} = n_{\rm os}$ to $n_{\rm cme} = n_{\rm os} + 0.1 \times i_{\rm max}$. In this study, $i_{\rm max}$ is 15, which is determined from our several trials. Other values (like 20 and 25) do not make any change to our results.

Step 5: From the set of synthetic CMEs in Step 4, we estimate the electron number density of the MPA sector,

$$\rho_{\rm cs}(r_{\rm sec}) = \frac{m_{\rm cs}(r_{\rm sec})}{V_{\rm cs}} \div m_e. \tag{5}$$

The mass of the MPA sector, $m_{\rm cs}$, is estimated from the total brightness measured in the synthetic CME and the assumption that all electrons lie on the plane of the sky. The volume of the MPA sector, $V_{\rm cs}$, is the same as that in Step 3.

Step 6: We estimate the rms errors between the observed density of the MPA sector, ρ_{os}, from Step 3 and the synthetic CME densities of the MPA sector, ρ_{cs}, from Step 5. The rms errors are calculated from the densities with $r_{\rm sec} > 10\,R_\odot$. Then we determine $n_{\rm cme}$, where the rms error is minimized.

Step 7: Using $n_{\rm cme}$ determined in Step 6, we estimate the CME mass, $M_{\rm cme}$, from the following equations,

$$M_{\rm cme} = \int_{\rm cone} \rho_{\rm cme}(r) dV \times m_e, \tag{6}$$

$$\rho_{\rm cme} = \rho_0 r^{-n_{\rm cme}}. \tag{7}$$

This volume integration takes place over the full volume of the full ice cream cone.

Step 8: We derive a conversion factor $C_{\rm o}$, which is a ratio of the synthetic CME mass $M_{\rm cme}$ to the observed CME mass $M_{\rm obs}$, which is given by

$$C_{\rm o} = \frac{M_{\rm cme}}{M_{\rm obs}}. \tag{8}$$

Using the above steps, we can estimate two kinds of the synthetic CME mass: (1) $M_{\rm cme1}$, which considers only the observed CME region, (2) $M_{\rm cme2}$ which includes both the observed CME region and the occulted area. The mass of the occulted area (hereafter an occulted mass) is estimated by the density distributions determined from the above steps but only considering the area whose radial distance is larger than $4\,R_\odot$. If we observe a limb CME in the LASCO C3 field of view, we can identify the CME structure over the occultation disk of LASCO C3. The below parts of the CME are still unknown. From this fact, we consider the area with $r > 4\,R_\odot$ when we calculate $M_{\rm cme2}$ from Equation (6). Of course, we can estimate all materials for $r > 1\,R_\odot$. However, our preliminary estimation for several cases shows that conversion factors seem to be too overestimated, which may be due to the assumption of the power-law distribution of electron number density.

From these masses, we derive two conversion factors: (1) $C_{\rm o1}$ is a ratio of the synthetic CME mass without the occulted mass to the observed mass, and (2) $C_{\rm o2}$ is a ratio of the synthetic CME mass with the occulted mass to the observed mass. To determine the conversion factors, we use a mass function given by

$$M(r) = M_{\rm c}(1 - e^{-r/h_{\rm c}}), \tag{9}$$

where r is the distance from the solar center, $M_{\rm c}$ is the final total mass, and $h_{\rm c}$ is the scale height (Colaninno & Vourlidas 2009). We obtain the final total mass, $M_{\rm obs}^{\rm c}$, $M_{\rm cme1}^{\rm c}$, and $M_{\rm cme2}^{\rm c}$, for the observation and the two synthetic CME by applying this function to the mass above $10\,R_\odot$ to minimize the effect of the occultation disk (e.g., Colaninno & Vourlidas 2009; Vourlidas et al. 2010).

3. Results and Discussions

We apply our method to 56 halo CMEs from 2000 January to 2014 September. The results of all events are summarized in Table 1. We generate synthetic CMEs based on the full ice cream cone structure produced using the three-dimensional parameters. Figure 3 shows the base difference images of the CME observed on 2014 September 10 and their corresponding synthetic CME images. As shown in the figure, the synthetic CME images are quite consistent with the observed ones.

Table 1
The Results from Our Method

LASCO Catalog		Full Ice Cream Cone Model					Power-law Exponent		Final Total Mass			Conversion Factor	
Date	Time (UT)	V_r (km s^{-1})	α (deg)	ϕ (deg)	θ (deg)	γ (deg)	n_{os}	n_{cme}	$\log(M^c_{obs})$	$\log(M^c_{cme1})$	$\log(M^c_{cme2})$	C_{o1}	C_{o2}
2000 Jan 18	17:54	1151	101	−7	76	74	2.7	3.1	15.9	16.2	16.4	2.0	3.2
2000 Feb 8	09:30	1557	77	−14	80	73	2.0	2.1	16.0	16.4	16.6	2.7	3.8
2000 Feb 17	21:30	840	141	−14	112	64	2.4	3.1	16.1	16.3	16.4	1.7	2.3
2000 Apr 4	16:32	1160	147	43	75	45	3.0	4.0	15.5	15.7	15.8	1.4	2.0
2000 Jun 6	15:54	1317	137	−11	94	78	1.5	1.7	16.4	16.7	16.8	1.8	2.1
2000 Jul 11	13:27	1660	92	−15	81	73	2.3	2.6	15.9	16.3	16.5	2.2	3.3
2000 Aug 9	16:30	991	93	−1	73	73	3.3	3.8	15.5	15.8	16.1	2.0	3.9
2000 Oct 2	20:26	755	84	−8	120	59	2.4	2.8	15.0	15.3	15.4	1.9	2.6
2000 Oct 25	08:26	1286	98	17	88	73	2.5	2.9	16.3	16.7	16.8	2.2	3.2
2001 Apr 6	19:30	1728	91	−12	110	67	2.0	2.3	16.2	16.5	16.6	2.3	3.0
2001 Apr 10	05:30	2240	125	17	106	67	2.3	2.8	16.3	16.6	16.7	1.8	2.4
2001 Apr 26	12:30	1473	82	−13	71	67	2.7	3.1	15.9	16.2	16.4	2.1	3.6
2001 Sep 28	08:54	1351	83	−9	106	72	2.2	2.2	16.2	16.6	16.7	2.6	3.6
2001 Oct 9	11:30	1197	124	0	119	61	2.6	3.3	16.2	16.5	16.6	1.7	2.5
2001 Oct 19	16:50	1318	104	7	80	78	3.0	3.4	15.9	16.2	16.5	2.0	3.3
2001 Nov 4	16:35	1867	155	30	87	60	1.8	2.5	16.6	16.8	16.9	1.6	1.9
2001 Nov 17	05:30	1654	137	−7	63	62	2.7	3.5	16.3	16.5	16.6	1.6	2.1
2002 Apr 17	08:26	1746	93	19	81	69	2.2	2.5	16.0	16.3	16.4	2.2	3.0
2002 May 22	03:50	2097	80	22	103	65	3.5	3.9	15.9	16.1	16.5	2.0	4.1
2002 Aug 16	12:30	1710	124	−15	114	62	2.5	3.0	16.3	16.5	16.7	1.8	2.5
2003 May 29	01:27	1794	87	27	97	62	2.2	2.6	15.6	15.9	16.0	2.1	2.8
2003 Aug 14	20:06	592	90	−5	81	80	1.5	1.6	15.5	15.9	16.0	2.8	3.4
2004 Jan 20	00:06	1369	119	18	90	72	2.3	2.8	16.1	16.4	16.5	1.9	2.5
2004 Jan 21	04:54	1077	106	−15	84	74	1.9	2.3	15.9	16.2	16.3	2.1	2.8
2004 Jul 20	13:31	1163	80	11	80	75	3.2	3.4	15.7	16.1	16.4	2.5	4.9
2004 Jul 25	14:54	1389	150	16	118	58	2.8	3.8	16.2	16.3	16.5	1.5	2.1
2004 Sep 12	00:36	1594	131	−16	95	73	2.8	3.5	16.3	16.5	16.7	1.7	2.5
2005 Jan 5	15:30	1049	76	−17	83	72	2.1	2.3	15.4	15.8	15.9	2.7	3.8
2005 May 26	15:06	769	130	2	100	80	2.7	3.3	15.6	15.9	16.1	1.8	2.6
2005 Aug 22	01:31	1076	116	25	95	65	2.7	3.4	15.8	16.1	16.2	1.7	2.6
2006 Jul 6	08:54	1179	67	14	105	70	2.5	2.6	16.2	16.6	16.9	2.6	4.4
2006 Aug 16	16:30	1138	96	−1	113	67	2.1	2.5	16.2	16.5	16.7	2.1	2.8
2006 Dec 14	22:30	1444	101	16	90	74	2.5	2.9	15.9	16.2	16.4	2.1	3.1
2010 Feb 7	03:54	475	142	−1	91	89	3.1	3.6	15.4	15.6	15.7	1.6	2.4
2010 Aug 14	10:12	869	100	44	102	45	3.2	4.2	15.6	15.7	15.9	1.5	2.3
2011 Mar 21	02:24	1297	130	17	68	62	3.1	4.0	16.1	16.3	16.5	1.5	2.4
2011 Jun 7	06:49	1513	90	5	106	73	2.6	2.9	16.0	16.3	16.5	2.3	3.7
2011 Aug 4	04:12	1898	110	8	68	67	2.7	3.3	15.9	16.2	16.4	1.8	2.6
2011 Aug 9	08:12	1560	119	57	89	33	2.0	2.6	15.7	15.9	16.0	1.5	1.8
2011 Sep 22	10:48	2406	111	−41	110	45	2.7	3.1	16.2	16.4	16.5	1.5	2.1
2011 Nov 26	07:12	1107	123	42	73	45	2.4	3.3	16.0	16.2	16.3	1.5	2.0
2012 Jan 23	04:00	3254	72	3	67	67	2.6	2.9	16.2	16.5	16.7	2.3	3.9
2012 Jan 27	18:27	2956	79	22	69	60	2.5	3.0	16.3	16.6	16.8	1.9	3.1
2012 Mar 13	17:36	2855	66	20	77	66	2.6	2.8	16.1	16.4	16.7	2.4	4.2
2012 May 17	01:48	2516	63	20	90	70	2.3	2.4	16.1	16.6	16.8	2.8	4.4
2012 May 26	20:57	2969	63	29	82	60	3.2	3.4	15.4	15.7	16.0	2.0	4.0
2012 Jun 14	14:12	1351	138	6	97	81	1.8	2.1	16.0	16.3	16.3	1.8	2.1
2012 Jul 2	08:36	1827	75	−25	90	65	2.5	2.7	15.9	16.2	16.4	2.2	3.6
2012 Jul 23	02:36	2934	77	22	85	67	2.5	2.7	16.1	16.5	16.7	2.3	3.7
2012 Aug 31	20:00	1634	118	−34	93	56	2.6	3.3	16.2	16.4	16.6	1.6	2.5
2012 Sep 28	00:12	1439	101	14	90	76	2.9	3.3	15.9	16.2	16.4	2.1	3.6
2012 Nov 20	12:00	1460	62	19	91	71	2.2	2.2	15.6	16.1	16.3	3.0	4.5
2013 Apr 11	07:24	1203	146	−9	94	80	2.2	2.7	16.2	16.4	16.5	1.7	2.1
2014 Apr 2	13:36	2519	55	−14	74	69	2.7	2.7	16.1	16.5	16.7	2.9	4.7
2014 Apr 18	13:25	1527	130	16	103	69	2.3	2.8	16.1	16.4	16.5	1.7	2.3
2014 Sep 10	18:00	1950	88	9	82	78	2.4	2.6	16.2	16.6	16.8	2.5	3.7

Note. The first two columns give the information of the CMEs: date and time of the first appearance in the SOHO/LASCO C2 field of view. Columns 3–7 are the three-dimensional parameters obtained from the full ice cream cone model: the radial velocity V_r, the angular width α, the longitude ϕ of the source region, the colatitude θ of the source region, and the inclination angle γ between the cone axis and the plane of the sky. Column 8 is the power-law exponent of the density of the MPA sector from the observation (n_{os}). Column 9 is the power-law exponent of synthetic CME density (n_{cme}). Column 10 is the final total mass from the observations (M^c_{obs}). Columns 11–12 show the final total mass of the synthetic CMEs without the occulted mass (M^c_{cme1}) and that with the occulted mass (M^c_{cme2}), respectively. Column 13–14 present the conversion factors (C_{o1} and C_{o2}) from the synthetic CME mass without the occulted mass and that with the occulted mass, respectively.

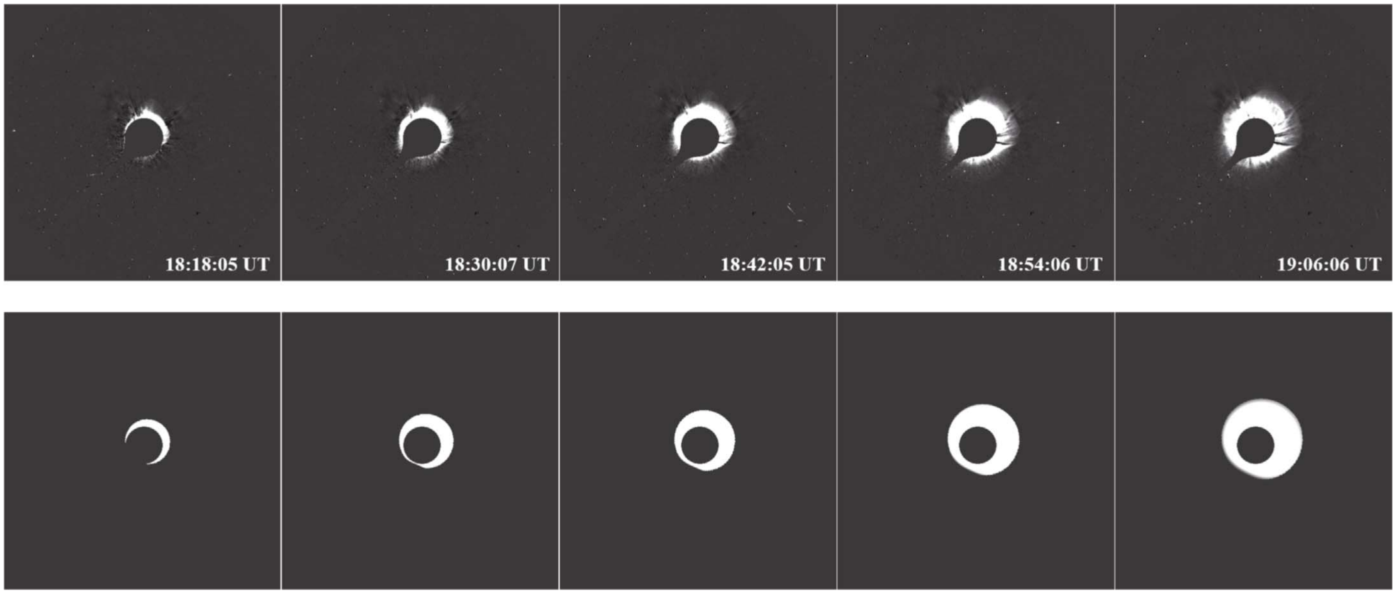

Figure 3. Top panels: the base difference images of the CME observed on 2014 September 10 by SOHO/LASCO C3. Bottom panels: their corresponding synthetic CME images generated by our method.

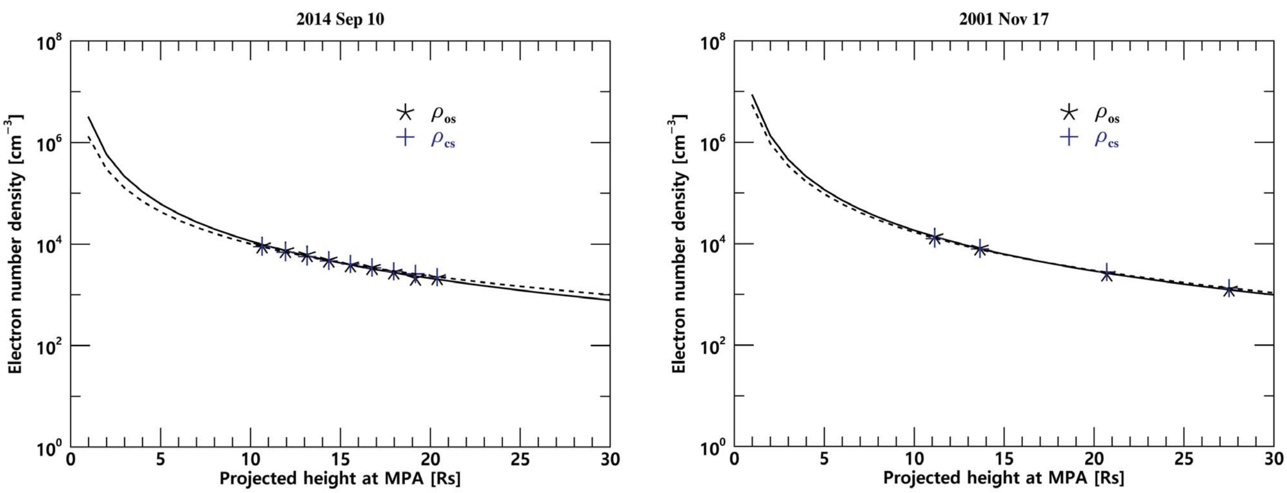

Figure 4. Density profiles of the MPA sector with projected height for the 2001 November 17 event (a) and the 2014 September 10 event (b). The asterisk and plus symbols are the density distribution from observations and the synthetic CMEs, respectively. The solid and dashed lines are the density fitting line by a power-law fit from the observations and the synthetic CMEs, respectively.

To determine the electron number density distribution of the synthetic CME corresponding to observations, we minimize the rms error between the densities of the MPA sector from the observation and the synthetic CMEs. Figures 4(a) and (b) show the density distributions at the MPA sector of the observation and the synthetic CME with projected height for the events on 2001 November 17 (hereafter event 1) and 2014 September 10 (hereafter event 2), respectively. The density distributions of the MPA sector from the observations approximately follow power laws with the exponent ($n_{\rm os}$) of 2.7 for event 1 and 2.4 for event 2. For all 56 events, the power-law exponent $n_{\rm os}$ of the density at the MPA sector for the observations ranges from 1.5 to 3.6 and its average is about 2.5. We find that the density distributions of the MPA sector from the synthetic CMEs are very similar to the observations, as shown in Figures 4(a) and (b). This fact implies that the power-law assumption for CME density is enough to generate the synthetic CME corresponding to the observation. From this minimization, we find that the electron number densities of the synthetic CMEs follow the power-law distributions with the exponent ($n_{\rm cme}$) of 3.3 for event 1 and 2.6 for event 2, respectively. On average, the density distributions of the synthetic CMEs for all 56 events follow the power-law with the exponent ($n_{\rm cme}$) of 2.9.

Figures 5(a) and (b) present the observed mass ($M^{\rm c}_{\rm obs}$) and two synthetic CME masses (the synthetic CME mass without the occulted mass $M^{\rm c}_{\rm cme1}$ and the synthetic CME mass with occulted mass $M^{\rm c}_{\rm cme2}$) for event 1 and event 2 as a function of radial height, respectively. For $M^{\rm c}_{\rm cme2}$, we note that the occulted mass does not include all mass that is behind the occultation disk because we consider the area with $r > 4\,R_\odot$ as mentioned in Section 2.2. We find that the synthetic CME mass based on the power-law density distribution converges to a constant value, which is similar to the observed mass. From the observations, the final total mass, $M^{\rm c}_{\rm obs}$, is obtained as $10^{16.3}$ g

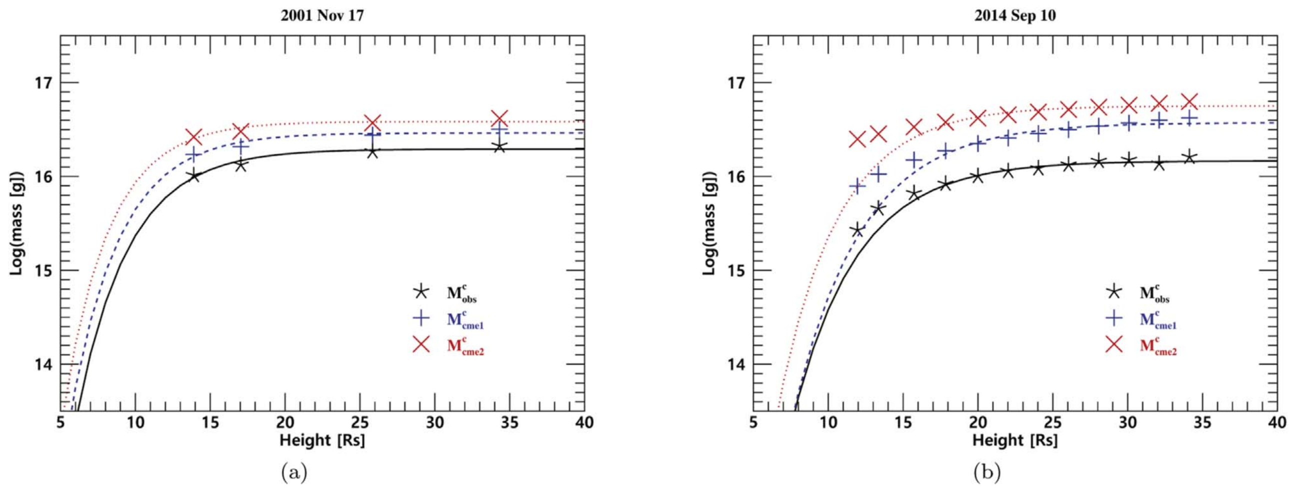

Figure 5. CME mass distributions with height for the 2001 November 17 event (a) and the 2014 September 10 event (b). The asterisk, plus, and cross symbols represent the observed mass, the synthetic CME mass without the occulted mass, and the synthetic CME mass with the occulted mass, respectively. The solid, dashed, and dotted lines are the fitting lines by Equation (9) for the observed mass and the two synthetic CME mass, respectively.

for event 1 and $10^{16.2}$ g for event 2. For event 1, the synthetic CME mass without the occulted mass, $M^{c}_{\rm cme1}$, and the synthetic CME mass with the occulted mass, $M^{c}_{\rm cme2}$, are $10^{16.5}$ g and $10^{16.6}$ g, respectively. For event 2, $M^{c}_{\rm cme1}$ and $M^{c}_{\rm cme2}$ are $10^{16.6}$ g and $10^{16.8}$ g, respectively.

For the two synthetic masses, we determine the conversion factors C_{o1}, which is a ratio of the synthetic CME mass without the occulted mass to the observed mass, and C_{o2}, which is a ratio of the synthetic CME mass with the occulted mass to the observed mass. For event 1, C_{o1} is 1.6 and C_{o2} is 2.1. For event 2, C_{o1} and C_{o2} are 2.5 and 3.6, respectively. For all 56 events, the conversion factor C_{o1} ranges from 1.4 to 3.0 and its average is 2.0. The factor C_{o2} ranges from 1.8 to 5.0 with an average of 3.0. These results imply that the observed halo CME mass can be underestimated by about 2 times when we consider the observed CME region and about 3 times when we consider the region including the occulted area. The result for the factor C_{o1} is similar to previous results of calculations (Vourlidas et al. 2000), MHD simulations (Lugaz et al. 2005), and stereoscopic methods (Colaninno & Vourlidas 2009).

We examine the dependence of the conversion factors from two types of synthetic CME masses on three-dimensional parameters of halo CMEs obtained from the full ice cream cone model. As a result, we find that these factors are not correlated with the radial velocity. The dependence of the two conversion factors on the inclination angle γ between the cone axis and the plane of the sky, which is defined as the equation $\sin\gamma = \sin\theta\cos\phi$, shows a week correlation (CC $= 0.46$ for C_{o1} and CC $= 0.37$ for C_{o2}). Figure 6 shows the dependence of the two conversion factors on angular width. The conversion factors have a very strong negative correlation with the angular widths of the halo CMEs (CC $= -0.82$ for C_{o1} and CC $= -0.88$ for C_{o2}). This fact means that a significant mass fraction of a halo CME with a larger angular width is closer to the plane of the sky than that with a smaller angular width.

Figure 7 shows the conversion factor as a function of inclination angle γ for the 2006 December 14 event whose angular width is 101°, which is close to the average value of angular widths. From the result, we find that the conversion factor increases as the central axis of the cone moves away from the plane of the sky. At $\gamma = 90°$, the CME mass is

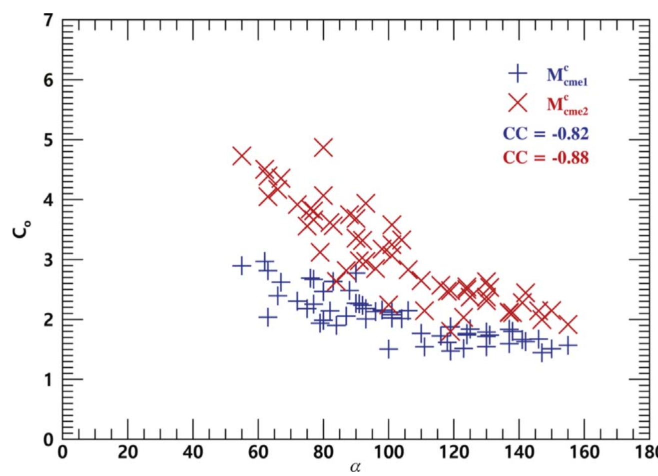

Figure 6. Conversion factor as a function of angular width. The plus and cross symbols are the factors from the synthetic CME mass without the occulted mass and the synthetic CME mass with the occulted mass, respectively.

significantly underestimated by a factor of about 2.4 for C_{o1} and about 3.5 for C_{o2}. It is noted that the conversion factor and its dependence on inclination angle depends on CME since each CME has its own electron number density distribution and three-dimensional parameters.

4. Summary and Conclusion

In this study, we have presented a new method to estimate the halo CME mass using a synthetic CME. To generate a synthetic CME, we assume a full ice cream cone model (Na et al. 2017) for CME structure and a power-law distribution for CME electron number density distribution. We apply this method to 56 halo CMEs observed by SOHO/LASCO from 2000 January to 2014 September. We find that the density assumption is reasonable from the comparison of the densities estimated at the MPA sector from the observation and the synthetic CME. On average, the synthetic CME density distributions follow the power law with an exponent of about 2.9. From the density distribution, we estimate two kinds of

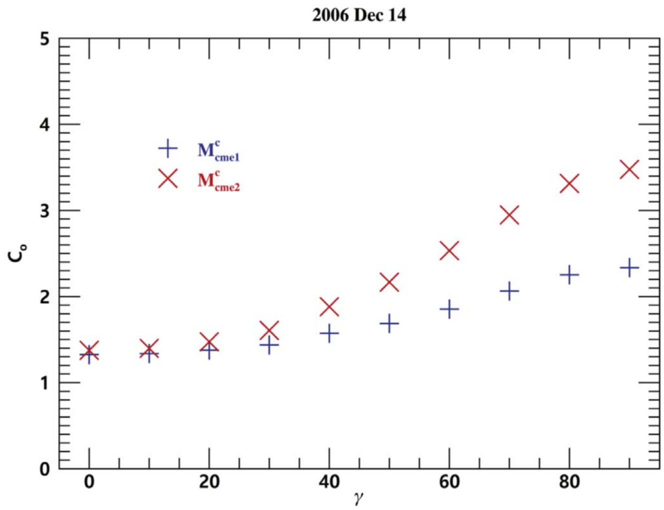

Figure 7. Conversion factor as a function of the inclination angle, which is between the cone axis and the plane of the sky, for 2006 December 14 event. The plus and cross symbols are the factors from the synthetic CME mass without the occulted mass and the synthetic CME mass with the occulted mass, respectively.

synthetic CME masses: (1) the synthetic CME mass without the occulted mass, and (2) the synthetic CME mass with the occulted mass. Then we obtain a conversion factor that is defined as a ratio of the synthetic CME mass to the observed mass. The average conversion factors for the synthetic CME mass without the occulted mass is 2.0, which is similar to the previous studies (e.g., Vourlidas et al. 2000; Lugaz et al. 2005; Colaninno & Vourlidas 2009). For the synthetic CME mass with the occulted mass, its average is 3.0, which is a new estimation of the CME mass with the occulted area. Since this case seems to be more reasonable than that without the occulted area, the CME mass, on average, is underestimated by a factor of about 3. Interestingly, we find that the conversion factors of halo CMEs have a very strong negative correlation with angular width.

From this study we have demonstrated the validity of our method for estimating the mass of halo CMEs. Our method can be extended in a couple of aspects. First, we can estimate the mass of any type of CME including halo CMEs using our method. Since it is particularly difficult to calculate an accurate mass for a halo CME, they have generally not been included in statistical investigations (e.g., Vourlidas et al. 2010; Aarnio et al. 2011). Our method will enable a more accurate statistical study of all CMEs. Second, if we determine the mass of CMEs more accurately, physical parameters derived from mass, such as kinetic energy, can be reasonably determined.

This work was supported by the BK21 plus program through the National Research Foundation (NRF) funded by the Ministry of Education of Korea, the Basic Science Research Program through the NRF funded by the Ministry of Education (NRF-2016R1A2B4013131, NRF-2019R1A2C1002634), the Korea Astronomy and Space Science Institute (KASI) under the R&D program "Study on the Determination of Coronal Physical Quantities using Solar Multi-wavelength Images (Project No. 2020-1-850-07)" supervised by the Ministry of Science and ICT, and Institute for Information & communications Technology Promotion (IITP) grant funded by the Korea government (MSIP) (2018-0-01422, Study on analysis and prediction technique of solar flares). The SOHO/LASCO CME catalog is generated and maintained at the CDAW Data Center by NASA and the Catholic University of America in cooperation with the Naval Research Laboratory. SOHO is a project of international cooperation between the ESA and NASA.

ORCID iDs

Hyeonock Na https://orcid.org/0000-0001-9528-1471
Yong-Jae Moon https://orcid.org/0000-0001-6216-6944
Jin-Yi Lee https://orcid.org/0000-0001-6412-5556
Il-Hyun Cho https://orcid.org/0000-0001-7514-8171

References

Aarnio, A. N., Stassun, K. G., Hughes, W. J., & McGregor, S. L. 2011, SoPh, 268, 195
Bein, B. M., Temmer, M., Vourlidas, A., Veronig, A. M., & Utz, D. 2013, ApJ, 768, 31
Billings, D. E. 1966, A Guide to the Solar Corona (New York: Academic)
Brueckner, G. E., Howard, R. A., Koomen, M. J., et al. 1995, SoPh, 162, 357
Colaninno, R. C., & Vourlidas, A. 2009, ApJ, 698, 852
Dai, X., Wang, H., Huang, X., Du, Z., & He, H. 2015, ApJ, 801, 39
de Koning, C. A. 2017, ApJ, 844, 61
Domingo, V., Fleck, B., & Poland, A. I. 1995, SoPh, 162, 1
Gosling, J. T., McComas, D. J., Phillips, J. L., & Bame, S. J. 1991, JGR, 96, 7831
Hildner, E., Gosling, J. T., Hansen, R. T., & Bohlin, J. D. 1975, SoPh, 45, 363
Howard, R. A., Michels, D. J., Sheeley, N. R. J., & Koomen, M. J. 1982, ApJL, 263, L101
Howard, R. A., Moses, J. D., Vourlidas, A., et al. 2008, SSRv, 136, 67
Howard, R. A., & Vourlidas, A. 2018, SoPh, 293, 55
Howard, T. A., & Tappin, S. J. 2009, SSRv, 147, 31
Kaiser, M. L., Kucera, T. A., Davila, J. M., et al. 2008, SSRv, 136, 5
Liewer, P. C., de Jong, E. M., Hall, J. R., et al. 2009, SoPh, 256, 57
Liu, Y., Davies, J. A., Luhmann, J. G., et al. 2010, ApJL, 710, L82
Lugaz, N., Manchester, W. B. I., & Gombosi, T. I. 2005, ApJ, 627, 1019
Michalek, G. 2006, SoPh, 237, 101
Mierla, M., Davila, J., Thompson, W., et al. 2008, SoPh, 252, 385
Millward, G., Biesecker, D., Pizzo, V., & de Koning, C. A. 2013, SpWea, 11, 57
Na, H., Moon, Y. J., & Lee, H. 2017, ApJ, 839, 82
Pluta, A., Mrotzek, N., Vourlidas, A., Bothmer, V., & Savani, N. 2019, A&A, 623, A139
Thernisien, A., Vourlidas, A., & Howard, R. A. 2009, SoPh, 256, 111
Vourlidas, A., Howard, R. A., Esfandiari, E., et al. 2010, ApJ, 722, 1522
Vourlidas, A., Subramanian, P., Dere, K. P., & Howard, R. A. 2000, ApJ, 534, 456
Xie, H., Ofman, L., & Lawrence, G. 2004, JGRA, 109, A03109
Xue, X. H., Wang, C. B., & Dou, X. K. 2005, JGRA, 110, A08103